Challenges in Naval Ship and Submarine Hydrodynamics

Thomas C. Fu, Ph.D.
U.S. Office of Naval Research
Arlington, VA 22203-1995
UNITED STATES OF AMERICA

thomas.fu@navy.mil

ABSTRACT

Maritime vessel design has always presented a unique set of technical and engineering challenges; so much so, the entire profession of Naval Architecture developed and continues to thrive. The need to develop and operate military warships presents additional challenges (e.g. shock and survivability) but also amplifies traditional naval architecture challenges, all the while also restricting the solution space. If one looks at the design of military sea platforms as an over constrained optimization problem, one soon realizes these competing requirements are what motivates our desire to improve the understanding of the physics driving platform performance. This hope goes beyond the mechanical, electrical, sensor, control, and weapon systems of Navy ships, but includes the hydrodynamics of the platform, propulsor, and control surfaces and the environment. For, except for physical attack, a naval platform interacts with the world through environmental and hydrodynamic forcing, that is the environment (waves, wind, and buoyancy/gravity) acts on the platform, and it acts on the environment (propulsor and control surfaces). Though most Computational Fluid Dynamics (CFD) codes are, in general, able to simulate these types of ship-generated flows, the details of the underlying physics still present a challenge. Separated flows are a distinct subset of these flows that remain a challenge.

Smooth-surface separated flows have been extensively studied, and the U.S. Office of Naval Research has funded several research campaigns focused on flow separation, as it is especially relevant to naval ship and submarine performance. This paper will describe these flows and summarize the more recent studies.

1.0 INTRODUCTION

The need to better understand the hydrodynamics of naval platforms was realized long ago. The first U.S experimental model basin built to test and develop “war vessels” was constructed by Admiral David W. Taylor in 1898, and the first U.S. Office of Naval Research organized Symposium on Naval Hydrodynamics was held on September 24-28, 1956. The concluding remarks in a paper by Cox and Maccoll (1958) state, ‘. . . it will be necessary to understand better the physical conditions at the point of separation. There is also a need for exact solutions with yawed bodies.” Smooth-surface separated flows still challenge our understanding. Figure 1-1a shows the separating flow on an axisymmetric body at moderate angle of attack, and Figure 1-1b shows a representative CFD calculation for a submarine making a steady turn to starboard. Though most CFD codes will, in general, be able to simulate these types of flows the details, including the actual location of the primary separation line, the location of the vortices, and the details of the secondary flow still remain a challenge, especially if one wants to include surface roughness and move to higher full-scale Reynolds numbers and Reynolds numbers near laminar to turbulent transition.

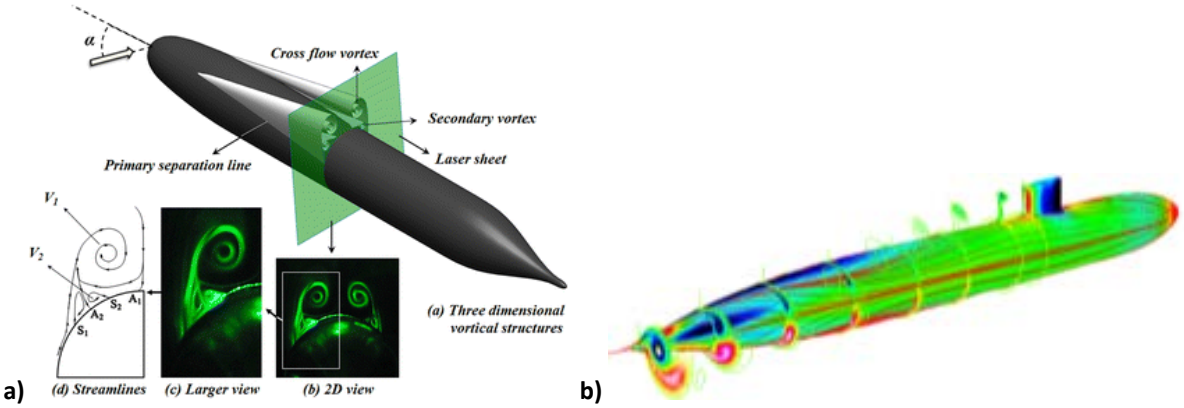

Figure 1-1: a) Sketch showing typical cross flow separation around an axisymmetric body (from Saeidinezhad et al, 2015), and b) a representative CFD calculation for a submarine making a steady turn to starboard.

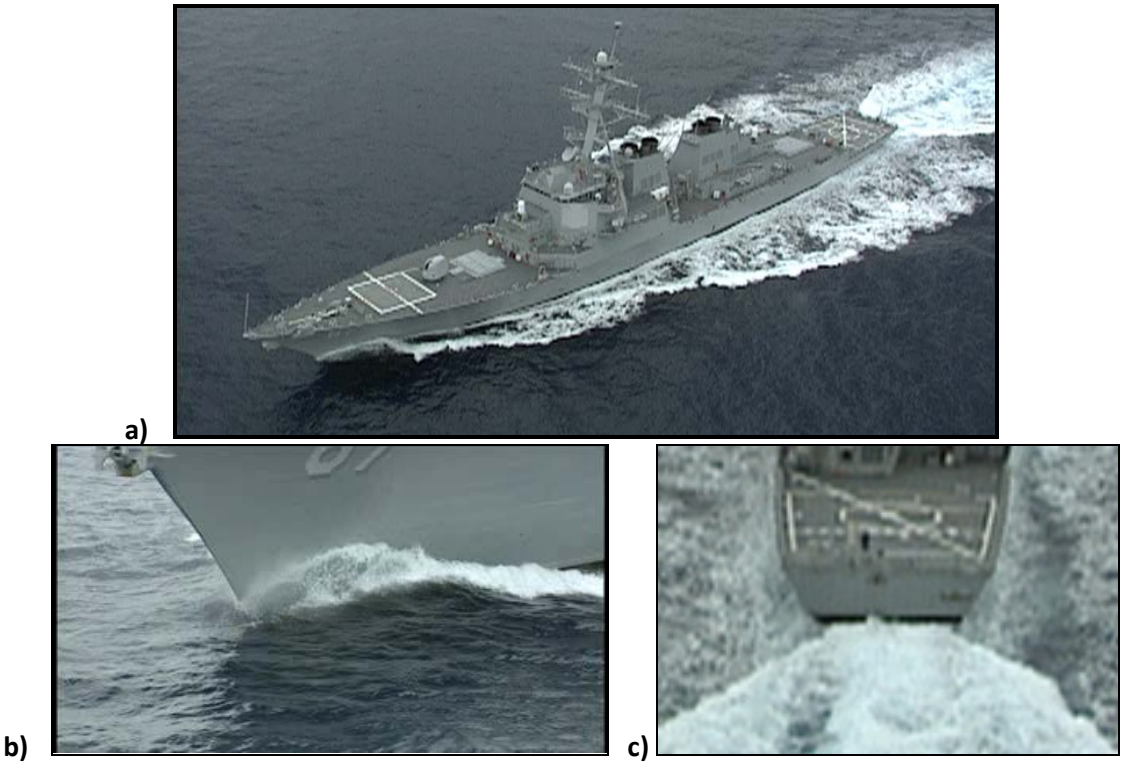

Figure 1-2: Image of a naval combatant and its hydrodynamics. Note the prominent breaking bow wave and c) the separated flow at the ship's transom.

Figure 1-2 shows a naval combatant moving at speed through relatively calm water. One can identify multiple flow phenomena that continue to challenge our understanding and ability to predict them accurately, including

the breaking bow wave and the separated flow at the transom. The addition of a realistic environment, unsteady wind and waves only adds to the difficulty. In fact, just the ability to accurately simulate a realistic wind field over a realistic wave field remains a topic of research. Figure 1-3 is an image of the ocean as the winds begin to build causing the waves to build, but also causing the waves to break. This is in fact a coupled problem with the flow separation of the wind over the waves inducing updrafts and downdrafts and is not a smooth-surface separated flow. This example is just to point out, that even as we make progress in understanding flow separation; there are still a number of additional affects that we continue to ignore.

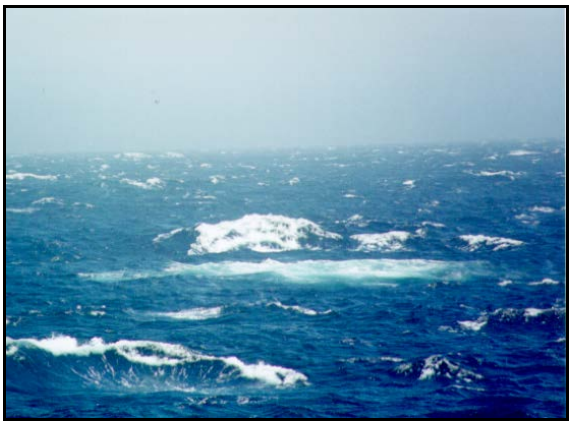

Figure 1-3: An image of the ocean as the winds begin to build causing the waves to build and break and inducing updrafts and downdrafts.

For this paper we will confine our discussion to just three canonical examples of smooth-surface separated flows, specific to the hydrodynamics of naval ships and submarines; cross-flow of an axisymmetric body, the flow off the transom of a surface ship, and the turbulent bow sheet.

2.0 CROSS-FLOW SEPARATION

Cross-flow separation continues to be a challenge for hydrodynamics and the location of separation is often a critical/limiting factor in the design and operation of naval platforms. A number of experiments have focused on identifying the separation line of a manoeuvring submarine and have extended back to the work on the DARPA SUBOFF (e.g. Ashok et al., 2015) model). Benchmark cross-flow separation studies have utilized the canonical 6:1 prolate spheroid geometry as a simple geometry that exhibits all the physics associated with cross-flow separation.

2.1 6:1 Prolate Spheroid

The 6:1 prolate spheroid has been long-standing viscous-flow benchmark geometry. An extensive review can be found in Andersson et al. (2018). Studies in the 1970s focused on the development of surface streamlines and critical point analyses methods and concepts of open and closed separation, including theoretical, experimental and numerical studies. In the 1990s NSWCCD towing tank flow-field PIV (Fu et al., 1994) and subsequent Virginia Tech wind tunnel surface shear stress and pressure and flow-field PIV (Wetzel et al., 1998) experiments

(Figure 2-2) enabled the development of theories and scaling (Lee, 2018) for cross flow primary and secondary separation.

Kim and Rhee (2003) utilized 6:1 prolate spheroid data to assess RANS turbulence models using near wall and wall function modelling. The k-ω and RS models performed best in qualitative prediction of the surface streamlines and flow field; however, all models fail to accurately predict lift and pitch moment for large incidence > 15 deg. Constantinescu et al. (2002) used the Virginia Tech surface pressure and skin friction data for assessment of RANS and DES. The results of both models are similar and show better qualitative agreement for 10 than 20 deg. Mor-Yossef (2015) and Karlsson and Fureby (2009) also used the Virginia Tech data.

Andersson et al. (2018) utilized a 6:1 prolate spheroid to study the low Re = 10-3000 flow using DNS for 45 deg. pitch building on previous studies for 90 deg. pitch. For Re ≤ 800, the wake is steady/laminar with symmetric vortex pairs. Studies for Re = 800, 1000 and 1200 show that an instability occurs for Re ≈1000 whereby the intermediate and far wake vortices become asymmetric with the weaker vortex deflected to the side with the stronger vortex. For Re = 1200 the weaker vortex rotates around the stronger vortex. For Re = 3000, the wake is almost fully turbulent with asymmetric vortex pairs not only in the intermediate and far but also in the near wake.

Table 2-1 summarize the experimental campaigns, which utilized a 6:1 prolate spheroid. Most of these studies focused on the three-dimensional boundary layer separation, with the Reynolds number range up to order ~4 x 10^6 . The angle of attack (AoA) range was 0 to 20 degrees, with the models typically tripped (no natural boundary layer transition). Most of the experiments were performed in air with just a few in water.

Table 2-2 summarizes the numerical studies, which utilized a 6:1 prolate spheroid. Typically, the flow has been computed using mainly RANS, but more recently some cases with DES and LES.

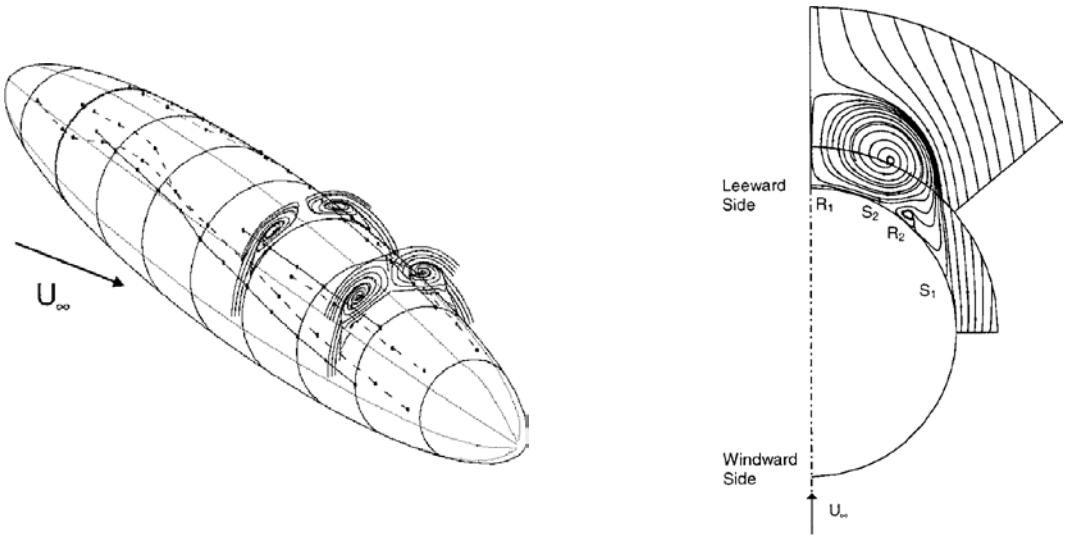

Figure 2-2. Simplified crossflow separation topology for a 6:1 prolate spheroid, α = 20 deg and *Re* = 4.5 x 10^6: a) three dimensional view; b) frontal view of secondary flow streamlines for x/L = 0.77 location in local model surface coordinates. Wetzel, T. G., Simpson, R. L., & Chesnakas, C. J. (2012). Measurement of three-dimensional crossflow separation. *AIAA Journal*, *36*(4), 557–564.
https://doi.org/10.2514/3.13861

Table 2-1. Summary of experimental campaigns, which utilized a 6:1 prolate spheroid geometry

Re Range	Angle of Attack	Tripping	Fluid Type	Method	Year and Author
11,700	3˚, 6˚, 10˚, 15˚, 20˚, 30˚		Water	Dyes and particles with laser sheet cuts	Costis., Hoang,& Telionis (1989)
1.4×10^6 4.2×10^6	0˚, 5˚,10˚, 15˚, 20˚	@ x/L ~ 0.1	Air	Surface oil flow visualization	Ahn & Simpson (1992)
4.2×10^6	10˚, 20˚		Air	LDV (3d fiber optics laser Doppler velocimetry)	Chesnakas & Simpson (1997)
4.2×10^6	10˚		Air	LDV	Chesnakas & Simpson (1994)
4.2×10^6	Pitch Up (0˚to 30˚within 0.33 sec)	@x/L =0.2	Air	Flush mount static and dynamic transducers and LDV	Hoang, Wetzel, & Simpson (1994)
4.2×10^6	2˚, 4˚, 6˚, 8˚, 10˚		Air	Flush mount static and dynamic transducers and LDV	Hoang, Wetzel, & Simpson (1994)
0.42×10^6 1.3×10^6 2.1×10^6	10˚to 20˚		Water	PDV	Fu et al. (1994)
4.2×10^6	Pitch Up (0˚to 30˚in 0.33s) Pitch up (0˚to 13.5˚in 0.25s)		Air	DyPPiR Model mount Hot film measurements	Wetzel & Simpson (1998)
4.2×10^6 6.5×10^6	10˚and 20˚		Air	Oil Flow Visualization (hot film meas. and LDV)	Wetzel & Simpson(1998)

Table 2-1. Summary of numerical studies, which utilized a 6:1 prolate spheroid geometry

Re Range	Angle of Attack	Tripping	Method	Year and Author
7.2 x 10^6 1.1 x 10^6	30˚		F3D thin-layer NS (Baldwin-Lomax with and without Deganni and Schiff crossflow modification, Johnson-King model with and without Degani-Schiff crossflow modification)	Gee, Cummings, & Schiff (1992)
4.2 x 10^6	10˚, 20˚.	at x/L =0.2	RANS and DES	Constantinescu et al. (2002)
4.2 x 10^6	0˚, 10˚, 20˚, 30˚ * Unsteady maneuvers		RANS with Spalart and Allmaras TCM (Turbulence closure model)	Rhee & Hino (2002)
4.2 x 10^6	10˚and 20˚		Large Eddy Simulation	Wikström et al. (2004)
10,000	90˚		DNS (Direct Numerical Simulation)	El Khoury, Andersson, & Pettersen (2010)
50, 200, 1,000	45˚		DNS (Direct Numerical Simulation)	Jiang, Gallardo, & Andersson (2014)
3,000	45˚		DNS (Direct Numerical Simulation)	Jiang et al. (2015) [16]
550 ~ 5,200	10˚and 20˚	at x/L =0.2	RANS (Reynolds Averaged NS), DES(Detached Eddy Sim), LES(Large Eddie Sim)	Fureby & Norrison (2019)
4,000	45˚			Strandenes et al. (2019)

3.0 TRANSOM FLOWS

Figure 1-2 shows a naval combatant moving at speed through relatively calm water. Figure 1-2c shows an image of the complex multiphase flow exiting from under the transom stern of the ship. Depending on the Froude number the transom can be wet (submerged) or dry (flow exists cleanly leaving the surface “dry”). This flow has been modelled in the lab, as the flow past a submerged vertical wall (Martínez-Legazpi, et al, 2013), see Figure 3-1.

a) 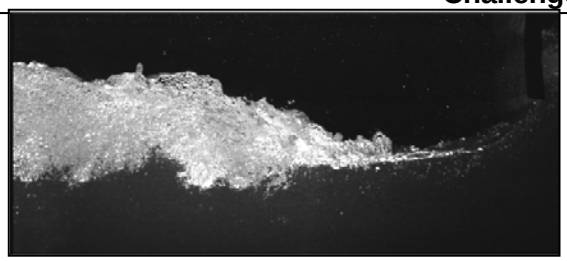 b) 

Figure 3-1: An image of the flow (right to left) past an inverted step, showing a simplified dry transom flow (courtesy of J. Lasheras); and b) the dry transom flow from a 1/8.25-scaled model of R/V Athena (Fu, et al, 2007).

3.1 R/V Athena /Model 5365

Full and model scale experimental measurements and Computational Fluid Dynamic (CFD) predictions of the wave-elevation topology behind a transom-sterned vessel, the R/V Athena 1 (Figure 3-2), were compared and assessed as part of an extensive ONR research campaign (Wyatt et al, 2008) to assess the capability of CFD to predict ship-generated wave fields (Terrill and Fu, 2008). Early in this program, prediction assessments were planned for both model-scale and full-scale of the stern wake for the R/V Athena. The model-scale measurements (Fu et al, 2007), CFD predictions, and assessments have been completed (Wilson et al, 2006).

Full-scale measurements of the free-surface elevation in the transom region of the R/V Athena I were made in early June of 2005 by research groups from the Scripps Institution of Oceanography-UCSD and the Naval Surface Warfare Center, Carderock Division (Fu et al, 2006). These measurements were made over a range of Froude numbers (see Table 3-1) covering both wet and dry transom conditions.

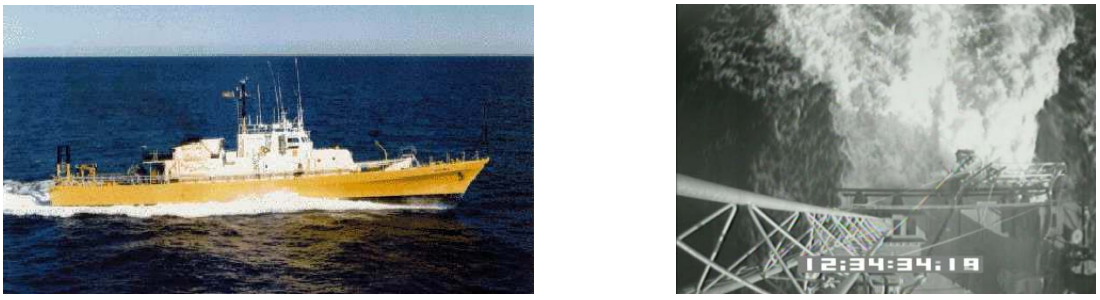

Figure 3-2: An image of the R/V Athena and the stern flow as viewed from the LIDAR tower.

Table 3-1: Test Conditions

Ship Speed (kts)	Ship Speed (m/s)	Fr_L	Fr_D
6	3.1	0.14	0.6
9	4.6	0.21	0.8
10.5	5.4	0.24	1.0
18	9.3	0.42	1.7
26	13.4	0.60	2.5

The sensors deployed for this experiment included the Quantitative Visualization (QViz) system, and a LIDAR sensor. The QViz system illuminates the surface of interest with a laser sheet and collects digital video images obtaining instantaneous cross sections of the spray envelope and surface profiles (Furey & Fu, 2002). In the R/V

Athena experiment the laser light sheet was projected onto the water surface perpendicular to the transom and moved incrementally from port to starboard to cover the transom area. The coverage area for the QViz system was 2.3 m (7.6 ft) (lateral) x 1.7 m (5.7 ft) (axial). The laser sheet was 1.7 m (5.7 ft) wide and incremented laterally at 30 cm (12 in) spacing. Two minutes of data were taken at each position, at 30 frames per second, resulting in 3600 frames at each of ten locations. Spatial accuracy and uncertainty was estimated to be approximately 0.2 cm. Figure 3-3 shows a typical set of wave profiles for a speed of 5.4 m/s (10.5 knots).

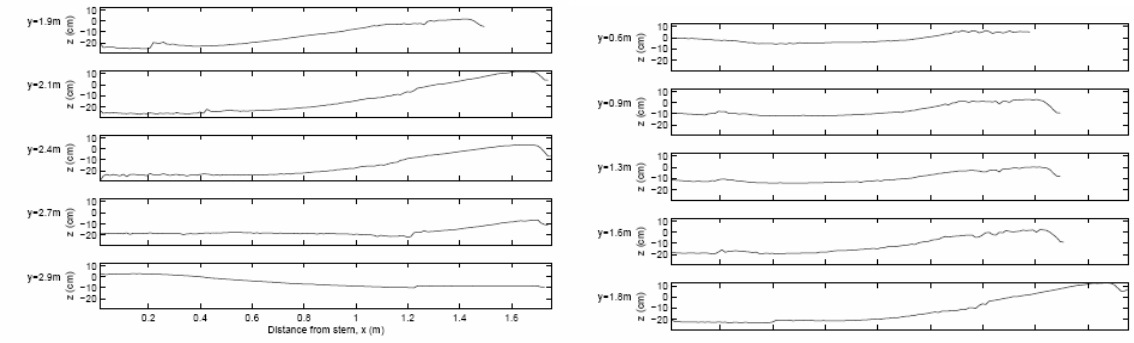

Figure 3-3: Profiles of free-surface elevations at 5.4 m/s (10.5 knots) at each of ten locations behind the stern.

The deployed LIDAR system consisted of a Riegl LMS-Q140I-80 LIDAR unit, an electronically controlled pan/tilt unit, a 6-DOF motion package, a tower-based mounting system, cabling, a bore-sited camera and a data acquisition and recording unit. The unit was mounted on the Athena transom. The coverage area for the LIDAR system was 6.1 m (20 ft) (lateral) x 0.3 cm (0.01 ft) (axial). Spatial resolution and accuracy was ~2:5 cm (~1 in), the sampling rate was from one to forty scans per second. Sixty seconds of data were taken at each speed for 900 frames. Figure 3-4 shows a typical set of results from the LIDAR system for a ship speed of 5.4 m/s (10.5 knots), Fr_L=0.24.

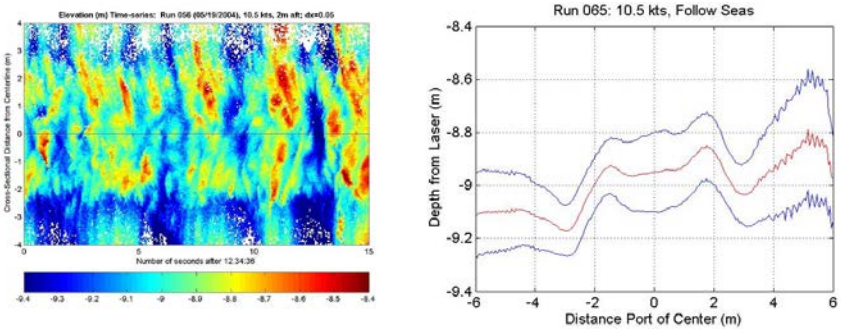

Figure 3-4: Sample result from the LIDAR measurement: a) Pseudo-color time-series of wave elevation at the stern of the R/V Athena. Ship speed is 10.5 knots (5.4 m/s), heading is head seas. b) Mean wake profiles (red) and standard deviation (blue) approximately 2.8 m aft of the stern at 10.5 knots (5.4 m/s) in following seas.

Measurements from these sensors were compared to numerical predictions from the following CFD codes: Das Boot, Numerical Flow Analysis, NFA, and CFDShip-IOWA. DasBoot is a nonlinear potential flow code with a breaking model (Wyatt, 2000). This code solves the fully-nonlinear hull and free-surface boundary conditions for a vessel traveling with steady speed on an undisturbed free surface (Wyatt et al, 2006). An empirically-derived model for transom-stern wave breaking for this code has been developed. Numerical Flow Analysis is a Cartesian grid formulation of the Navier-Stokes equations with a body force technique to impose the hull boundary conditions. A description of the code and its current capabilities can be found in Dommermuth et al, 2007. CFDShip-Iowa is an unsteady Reynolds-Averaged Navier-Stokes (URANS)/detached eddy simulation (DES) code that uses a single-phase level set method, advanced iterative solvers, conservative formulations, and the dynamic overset grid approach for free surface flows (Bhushan, et al, 2007).

Example comparisons between measurements and predictions for these three codes at model-scale are illustrated in Figure 3-5. Analysis of these data concluded that this suite of codes could predict the average transom wave height profile for both wet and dry transom conditions.

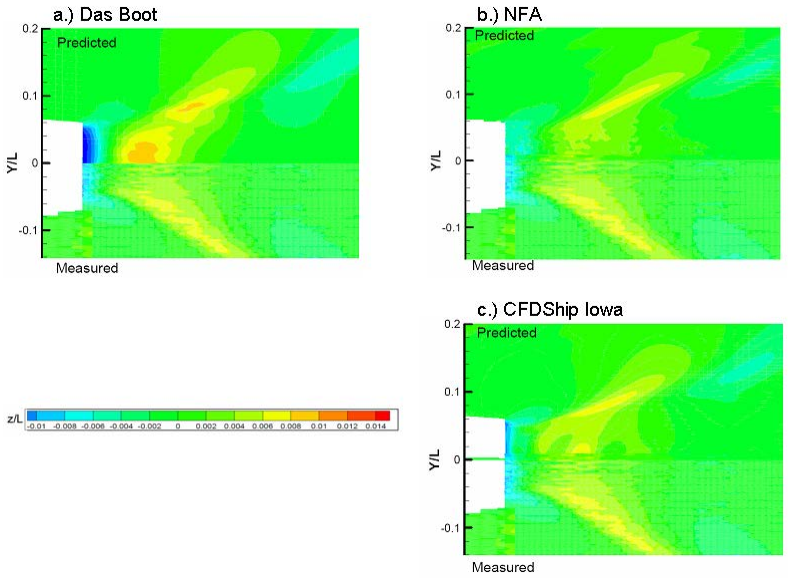

Figure 3-5: Example results of the computed stern flow for the R/V Athena at model scale for Fr_l=0.24, a) Das Boot, b) NFA and c) CFDship-Iowa (Bhushan et al, 2012).

3.2 Transom Model

To increase understanding of the turbulent multiphase flow associated with full-scale transom flow, detailed measurements were performed at the Naval Surface Warfare Center, Carderock Division, in 2007 and 2008 to investigate the breaking wave generated from a submerged ship transom in a repeatable setting (Drazen et al, 2010). The primary objective was to obtain full-scale qualitative and quantitative flow field data of a large breaking transom wave over a range of Froude numbers.

The experiments were conducted over two years. The first half provided an overview of the transom wake covering a range of draft Froude numbers. A more detailed study followed in the second year focusing on a subset of the conditions initially tested. Speeds of 5, 7, 8, and 9 knots were tested the first year with repeats at 7 and 8 knots the following year. Figure 3-6 shows a series of still images depicting the flow field aft of the transom for each speed. These speeds correspond to draft Froude numbers of 1.4, 1.9, 2.1, and 2.3 respectively. The literature suggests that a transom stern vessel will experience a dry stern at draft Froude numbers above 2.5 (Maki et al. 2007, Faltinsen 2005). A dry transom was observed starting at a slightly lower Froude number of 2.1.

A unique model (5673) was designed for this test. The model has a transom stern and was designed to minimize the generated bow wave so that the transom wave could be more effectively investigated. The model is 30 ft long with a maximum beam of 5 ft and a static transom submergence of 1 ft. The model was fixed in heave, but it was free to pitch. Block gauges were used to measure the lift, drag, and side forces on the model. Dynamic trim of the model was measured while underway using string potentiometers.

A variety of instrumentation was used to quantify the transom wake breaking wave. The shape of the transom wake was measured using a scanning LiDAR system, Quantitative Vizualization (QViz), ultrasonic wave height sensors, and a Nortek Acoustic Wave And Current profiler (AWAC). Velocity measurements within the wake from the AWAC were supplemented by measurements from a SonTek Acoustic Doppler Velocimeter (ADV). Void fraction probes and an optical bubble size imager were used to quantify air entrainment within the wake. Standard, high speed, and underwater video were also taken to supplement the other measurements. A fluorescent dye was used to provide insight into the flow path around the corner of the transom. Examples of the mean surface elevation of the wake at 7 and 8 knots are shown in Figure 3-7. Comparison of the data from 2007 and 2008 showed excellent agreement between measurements of the free-surface, see Figure 1-8. A contour plot of the void fraction aft of the transom at a speed of 8 knots is shown in Figure 3-9.

We show that a laboratory model capable of producing full-scale transom breaking waves similar to those of full-scale naval combatants is essential in obtaining high-quality detailed measurements of a transom breaking wave.

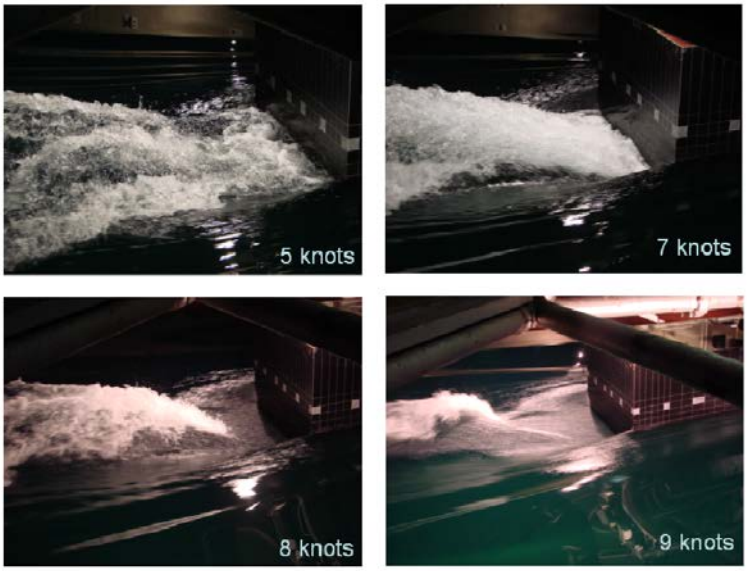

Figure 3-6: Still images depicting flow aft of transom at the various speeds tested.

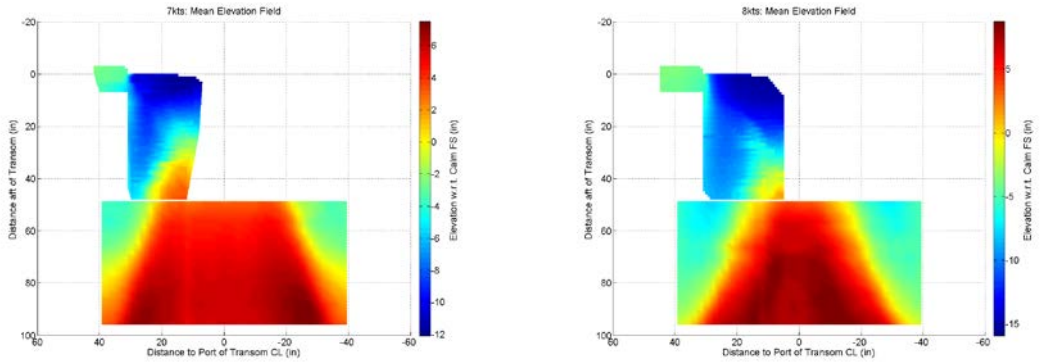

Figure 3-7: Comparison of the mean elevation of the free surface aft of the transom. The left hand side is at a speed of 7 knots and the right hand side is at 8 knots. Lower portion of each figure is data from the lidar while the top portion is from QViz.

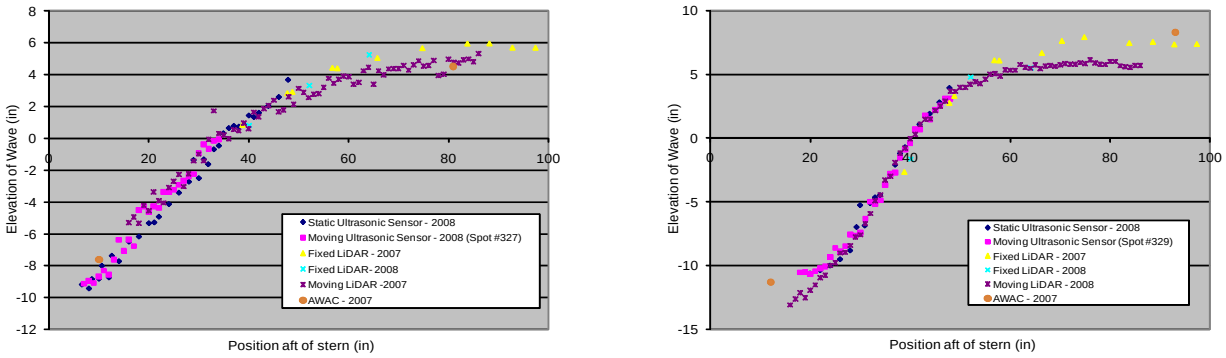

Figure 1-8: Comparison of the height of the wake aft of the transom as measured by a number of instruments.

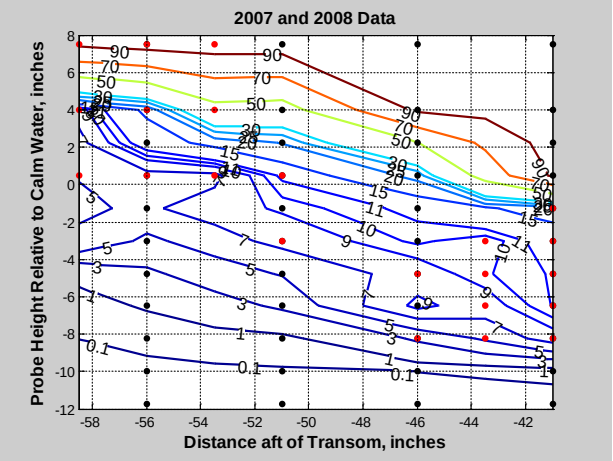

Figure 3-9: Contour plot of void fraction at a model speed of 8 knots. Black dots represent measurement locations from 2007 and red dots locations from 2008. A void fraction of 50% can be taken as a rough approximation of the free surface.

4.0 TURBULENT BOW SHEETS

a) b)

Figure 4-1: a) Image of the DDG-1000 and b) zoomed in on the turbulent bow sheet.

Over the past several years much progress has been made in computational fluid dynamics (CFD) and its ability to accurately simulate the hydrodynamics associated with a deep-V monohull planing craft (Fu et al., 2010 & 2012). This work has focused on not only predicting the hydrodynamic forces and moments, but also the complex multiphase free-surface flow fields, specifically the formation of the spray sheets, generated by a deep-V monohull planing boat at high Froude numbers. One of these state-of-the-art CFD codes is Numerical Flow Analysis, NFA (Dommermuth, et al., 2007; O'Shea, et al., 2008; and Brucker, et al., 2010). NFA solves the Navier-Stokes equations utilizing a cut-cell, Cartesian-grid formulation with interface-capturing to model the

unsteady flow of air and water around moving bodies. The turbulent thin fluid sheet generated at the bow of a naval combatant, see Figure 4-1, or high-speed planning craft is a unique smooth-surface flow separation problem as gravity plays a unique role in this type of flow, effectively peeling the flow from the hull/surface. To repeatedly generate this type of phenomena a series of wedge drop experiments was carried out. Numerical simulations of these experiments, undertaken by the Naval Surface Warfare Center, Carderock Division, NSWCCD and by the United States Naval Academy, USNA, Hydromechanics Laboratory, were performed using the computational fluid dynamics code Numerical Flow Analysis, NFA (Fu et al, 2014).

4.1 Experiments

In the NSWCCD testing (Lesar et al, 2012; Jiang et al, 2012) the wedge was dropped from rest from two heights, 15.24 cm (6 in) and 25.4 cm (10 in), above the undisturbed free surface. The model tank was 4.6 m (15 ft.) wide by 7.3 m (24 ft.) long by 4.4 m (14 ft. 6 in) deep. The wedge weighed 75 kg (165.2 lbs.) and was 91.4 cm (36 in) by 0.60 cm (23.75 in) with a deadrise angle of 10.23 degrees. Figure 4-2 shows the bottom of the instrumented wedge. Two symmetric pressure probes were located at 3.8 cm (1.5 in) from the keel. A four by four array of pressure probes had lines of four probes at 13.68, 17.26, 20.84, and 24.42 cm (5.385, 6.795, 8.205, and 9.615 in) from the keel. Each probe in the array was 3.58 cm (1.41 in) from its neighbor longitudinally and transversely.

Figure 4-2: Photograph of instrumented wedge used in NSWCCD experiment.

The USNA experiment utilized a larger number and wider range of drop heights (from about 7.6 cm (3 in) to 50.8 cm (20 in) above the waterline). Wedge position data, pressure data (PCB® sensors at six locations located from keel toward the chine and Tekscan® tactile pressure mat), acceleration data, and subsurface video were all acquired providing a detailed data set of short duration hydrodynamic impacts. The specific drop heights are 7.94, 12.7, 15.88, 25.4, 31.75, 38.1, and 50.8 cm (3.125, 5.0, 6.25, 10.0, 12.5, 15.0, and 20.0 in). The wedge was made from 1.3 cm (0.5 in) thick acrylic plates and had a deadrise angle of 20°. Vertical position vs. time, acceleration (tri-axial) vs. time, pressure maps, point pressures, and high-speed video were recorded for each drop height. Figure 4-3 shows the wedge and the notional design dimensions. The as built wedge was measured and found to be slightly misaligned with a beam at the lower edge of 30.34 cm (11.945 in) and 30.58 cm (12.04 in) at the upper edge. The height from the chine was also only 30.78 cm (12.125 in) not 64 cm (25 in) as shown in Figure 4-3. This misalignment also resulted in a model asymmetry with two different deadrise angles, 18 and 20 degrees.

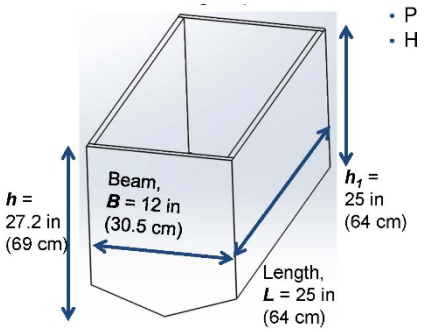

a)

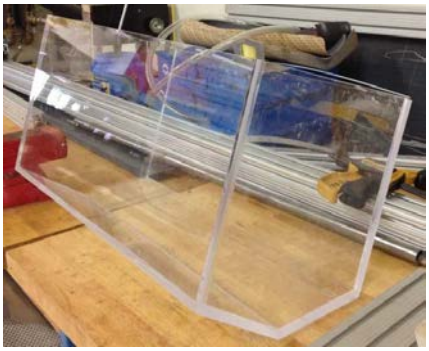

b)

Figure 4-3: a) Original notional wedge design and b) photograph of the wedge used in USNA experiment.

4.1 Code Assessment

Figure 4-4 shows the NFA simulation's geometry and computational domain. For both drop heights the NFA simulations used wall boundary conditions in each Cartesian direction. The number of grid points in the x, y and z directions was 1536, 1024, and 512, resulting in 805 million cells. Grid spacing near the wedge was 0.001L or 0.09 cm (0.035 in), where L is the wedge length. The non-dimensional time step taken was 0.00005, resulting in an output frequency of 37.8 KHz. The simulations were run a Cray XT5, on 768 processors and took 12 hours for the 15.24 cm (6 in) drop height, running for 2000 time steps, and 32 hours for the 25.4 cm (10 in) case, running 6000 time steps.

The output from the pressure probes is plotted against the pressure sampled from NFA in Figures 4-5 and 4-6 for the 15.24 cm (6 in) and 25.4 cm (10 in) drop heights respectively. The x axis is time in seconds and the y axis is gauge pressure in psi. Pressure-time histories from three completely separate drops are plotted together, with the peak from the first row of gauges aligned. The dashed black lines show 5 peaks in time, the first from the symmetric keel gauges and the remaining four from the four rows of pressure gauges in the array. Since the pressure pulse is quasi-2D each row of pressure gauges in the keel-wise direction shows approximately the same time history. The time histories exhibit variability associated with minor experimental irregularities. Because only three drops were performed at each height a detailed uncertainty analysis was not performed. To aid the reader blue error bars representing the minimum and maximum of the experimental peaks for the 3 drops are shown. The sampling frequency of the pressure probes was 19.2 KHz, while NFA pressures were extracted at a rate of 37.8 KHz.

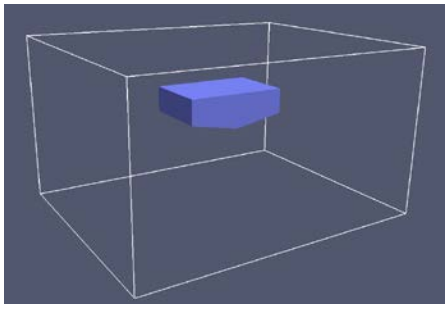

Figure 4-4: Image showing the NFA simulation's NSWCCD wedge geometry and computational domain.

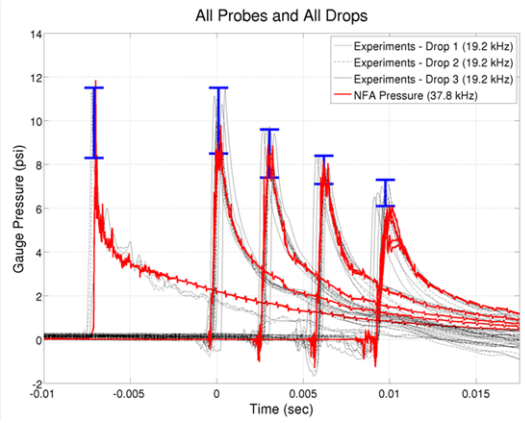

Figure 4-5: NSWCCD Assessment - Results of the 15.24 cm (6 in) drop height case - NFA pressure predictions plotted on top of pressure gauge output from 3 separate drops.

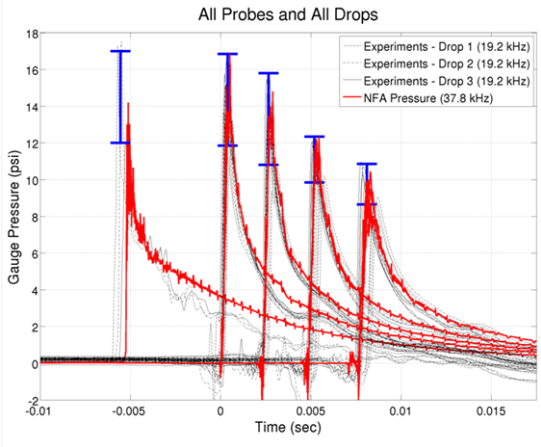

Figure 4-6: NSWCCD Assessment - Results of the 25.4 cm (10 in) drop height case - NFA pressure predictions plotted on top of pressure gauge output from 3 separate drops.

The peak from NFA's first row of gauges was aligned to the peak from the experiments and plotted in red. NFA shows excellent agreement for peak pressure magnitudes and pulse duration. The spray root takes approximately ten milliseconds to travel across the array of gauges and each peak pressure is maintained for less than 1 ms. The propagation in time of the pressure pulse from the spray root is slowed by the deceleration of the wedge due to the impact with the free surface. The length of time between the final two peaks is therefore greater than that of the preceding peaks. NFA correctly predicts this momentum transfer and thus the position in time of all four pressure peaks. NFA results are within the experimental variability for peak pressure and timing. It is notable that NFA also predicts the brief negative pressures seen in the experiments before the peak pressure due to the turbulent breakup of the expanding spray root.

Figures 4-7 and 4-8 show image sequences from the 15.24 cm (6 in) and 25.4 cm (10 in) drop height simulations respectively. The camera is looking up at the wedge from underneath the water surface. The wedge is painted with contours representing the pressure that NFA has calculated. Blue represents zero pressure while red indicates 103.4 kilopascals (15 psi). The pressure pulse can be seen moving outboard from the keel over the pressure probes indicated by white dots on the bottom of the wedge on the right side. This pulse is concentrated at the spray root which can be seen as the translucent surface that begins to break up later in the simulation.

As with the previous NSWCCD comparison, care was taken to ensure boundary condition and initial conditions matched the experimental setup when possible. The wedge geometry used for the initial simulations was the symmetric, notional design geometry, not the as built geometry. The wedge was positioned at the same distance from the close side of the tank as in the experiments, 1.07 m (42 in). The other sides of the tank were set at two body lengths away from the wedge and this position was found to be far enough to not impact the initial pressure wave and spray root. A course simulation done with the walls at 4 body lengths away produced similar results. The experiment was done in a large tank and the actual dimensions would have been unrealistic to model. The drop height of 0.3175 m (12.5 in) was chosen for the comparison since that case had the largest amount of high quality experimental measured data from the USNA test.

Table 1 provides details of how the computational domain has been distributed over the processors of the parallel computer. The multiplication of the number of subdomains in the X, Y and Z directions gives the total number of CPUs used, since each processor gets one subdomain. The multiplication of the number of cells per subdomain results in the total number of cells each processor works on. Finally, the number of cells in each coordinate direction multiplied together gives the total number of discrete cells in the simulation.

Table 4-1: USNA Simulation Computational Size

	X	Y	Z	Total
Subdomains	6	6	13	468
Cells	128	128	64	1,048,576
Total Cells	768	768	832	490,733,568

Figure 4-9 shows the NFA simulated pressure painted on the bottom of the wedge. The white dots represent the locations of the experimental probes installed on the side opposite of the close tank edge. The pressure wave is seen traveling out and over the probes in a similar fashion to previous wedge drop simulations. The pressure on the NFA panels representing the probe were then extracted and plotted versus time. A comparison between the NFA and experimentally measured pressure is presented in Figure 4-10. The NFA pressure data was aligned so that at time equal to zero the tip of the keel is impacting the free surface. The experimental data was processed similarly.

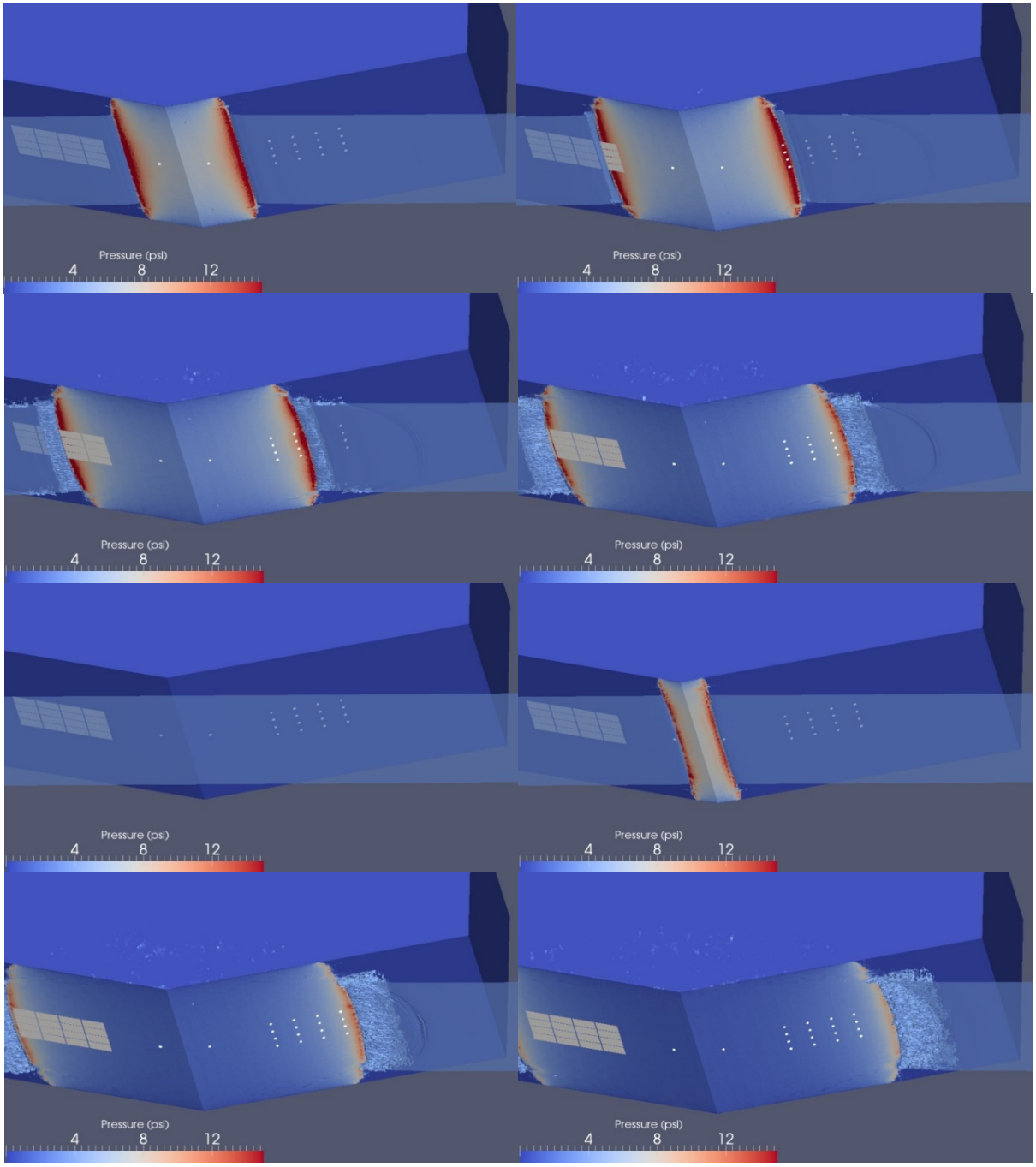

Figure 4-7: NSWCCD Assessment - Sequences of frames from an animation of the 15.24 cm (6 in) drop height wedge impacting the free surface. Pressure is interpolated onto the wedge and displayed, blue indicating 0 pressure, and red indicating 103.4 kilopascals (15 psi). Note the pressure wave from the spray root expanding transversely over the pressure gauges.

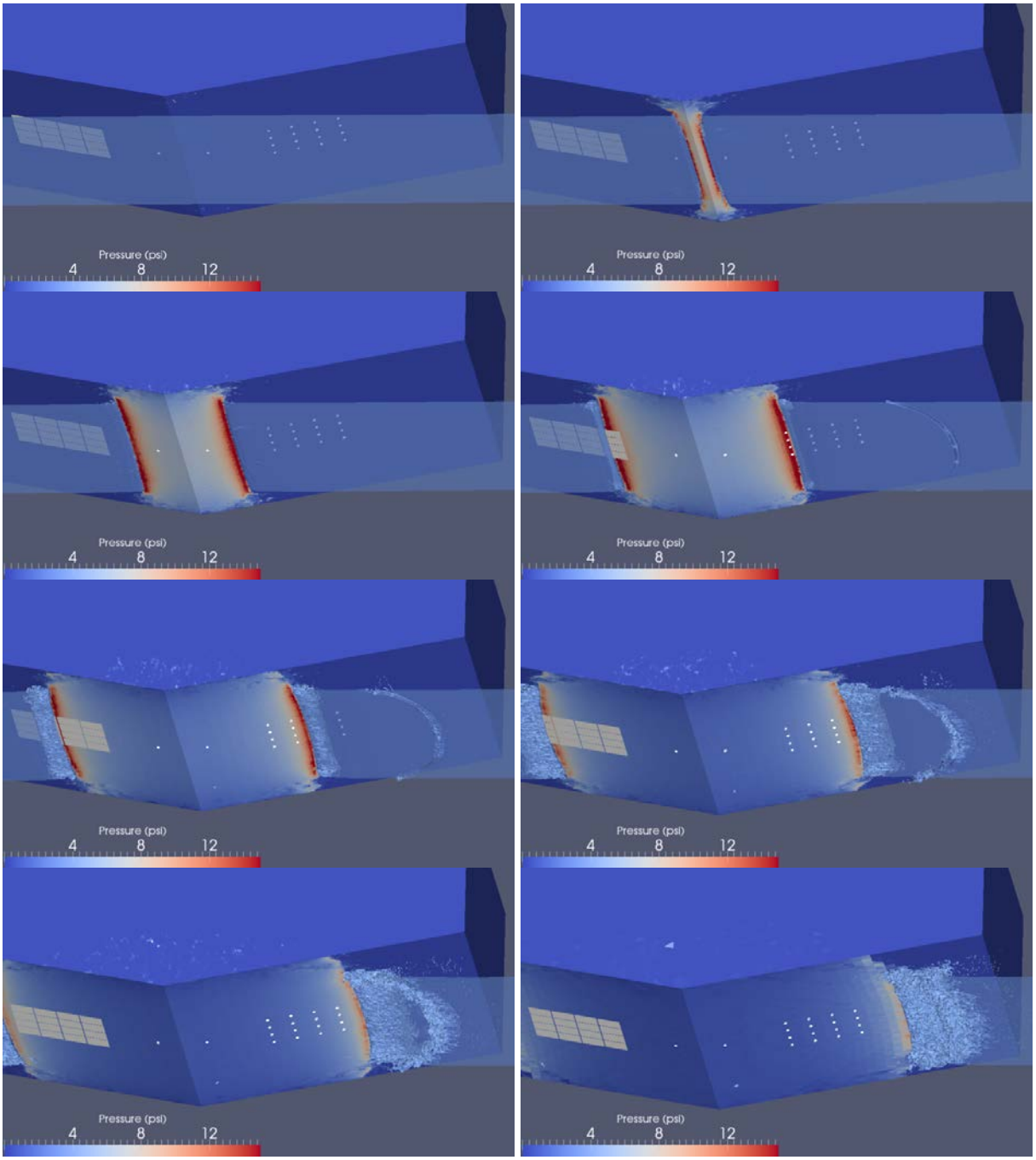

Figure 4-8: NSWCCD Assessment - Sequences of frames from an animation of the 25.4 cm (10 in) drop height wedge impacting the free surface. Pressure is interpolated onto the wedge and displayed, blue indicating 0 pressure, and red indicating 103.4 kilopascals (15 psi). Note the pressure wave from the spray root expanding transversely over the pressure gauges.

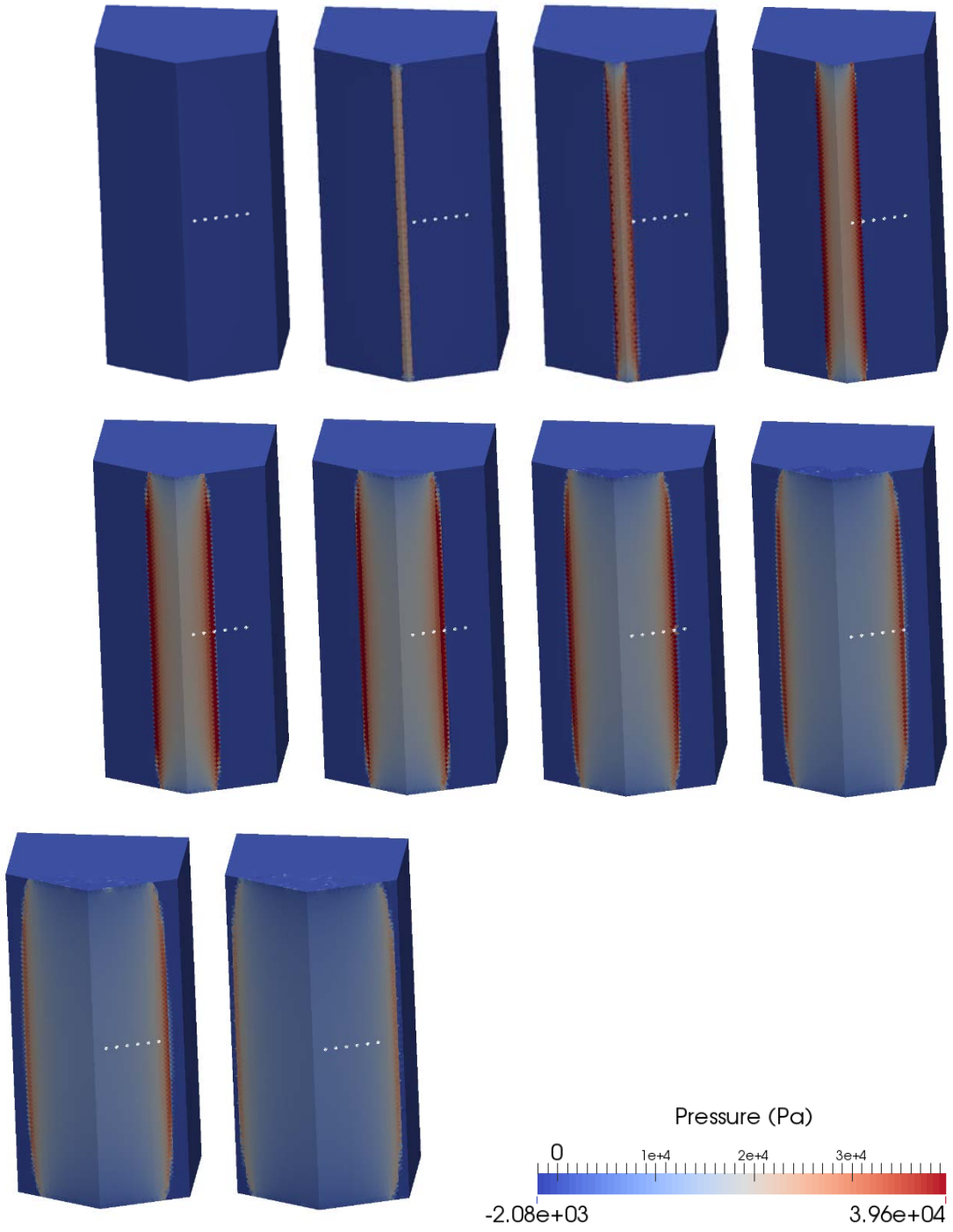

Figure 4-9: USNA Assessment - NFA simulated pressure values painted on the bottom of the USNA wedge at various times throughout the simulation for the 31.75 cm (12.5 in) drop height case.

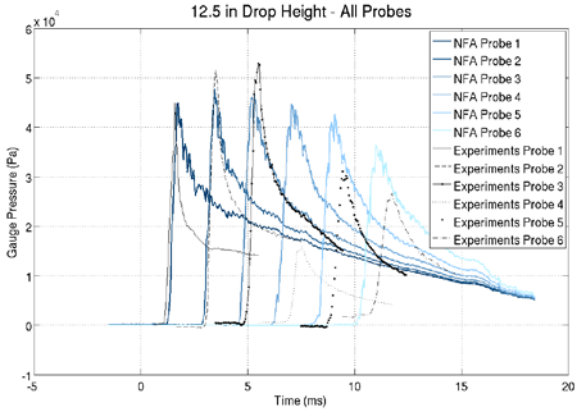

Figure 4-10: USNA Assessment - Results of the 31.75 cm (12.5 in) drop height case - NFA pressure predictions plotted on top of pressure gauge output.

The NFA pressure history for the probe closest to the keel matches well in run up and peak pressure to the experimentally measured values. It should be noted that the post peak pressure decay in the experimental probes is affected by thermal drift and is not accurate. For the next two probes, the pressures are under-predicted by NFA. The time between peaks is also slightly expanded in the NFA simulation. The fourth probe is inconsistent with the other probes and can be ignored. The final two probes are over-predicted by NFA.

5.0 SUMMARY

We discussed and gave examples of three canonical smooth-surface separated flows of naval importance as they directly affect naval ships and submarine performance. These three flows are:

1. Cross-flow separation of an axisymmetric body – the specific location and position of the shed vortices directly effects platform stability and manoeuvrability.
2. Separating flow off the transom of a surface ship – directly influences a surface ship's resistance, stability, and manoeuvrability.
3. The turbulent bow sheet – directly influences a surface ship's resistance, stability, and manoeuvrability.

ACKNOWLEDGEMENT

Many people contributed text and insight to this effort. Their contributions are appreciated, and any errors are mine. Those whose efforts are directly reflected in this work are: Steve Ceccio, Fred Stern, David A. Drazen, Anne M. Fullerton, Kristine Chevalier, David Jeon, Donald Wyatt, Genevieve L. Taylor, T. Xing, Eric Terrill, Thomas O'Shea, Kyle Brucker, Carolyn Judge, Christine Ikeda, and Doug Dommermuth. Much of this work was and is supported by the U.S. Office of Naval Research (ONR), program managers: Dr. Robert A. Brizzolara Dr. Steve Russell, Dr. Paul Hess, Dr. Ki-Han Kim, and Dr. L. Patrick Purtell.

REFERNCES

[1] Ahn, S., & Simpson, R. (1992). Cross-flow separation on a prolate spheroid at angles of attack. https://doi.org/10.2514/6.1992-428

[2] Ashok A., Van Buren T., ands Smits A.J. (2015**)**. "Asymmetries in the wake of a submarine model in pitch," *J. Fluid Mech.* 774, 416–442.

[3] Andersson, Jiang, and Okulov, (2018). Computational Modeling of Bifurcations and Instabilities in Fluid Dynamics (A. Gelfgat ed.), Springer.

[4] Bhushan, S., Xing, T., Carrica, P., & Stern, F., (2007). "Model and Full-Scale URANS/DES Simulations for R/V Athena Resistance, Powering and Motions," 9th Int. Conf. on Num. Ship Hydro., Ann Arbor, MI, Aug. 5-8

[5] Bhushan, S., Xing, T. and Stern, F. (2002). "Vortical Structures and Instability Analysis for Athena Wetted Transom Flow with Full-Scale Validation," *ASME J. Fluids Eng.*, Volume 134, Issue 3, March, 031201 (18 pages).

[6] Brucker, K. A., O'Shea, T. T. and Dommermuth, D. G., (2010). "Numerical Simulations of Breaking Waves – Weak Spilling to Strong Plunging," Proceedings of the 28th Symposium on Naval Hydrodynamics, Pasadena, CA, September 12-17.

[7] Chesnakas, C. J., & Simpson, R. L. (1997). "Detailed Investigation of the Three-Dimensional Separation about a 6:1 Prolate Spheroid." AIAA Journal, 35(6), 990–999. https://doi.org/10.2514/2.208

[8] Chesnakas, C. J., & Simpson, R. L. (1994). "Full three-dimensional measurements of the cross-flow separation region of a 6:1 prolate spheroid". 17, 68–74.

[9] Constantinescu G. S., Pasinato H., Wang Y.-Q., Forsythe J. R., Squires K. D. (2002). "Numerical investigation of flow past a prolate spheroid." *J. Fluids Eng.* 124, 904–910, https://doi.org/10.1115/1.1517571.

[10] Costis, C. E., Hoang, N. T., & Telionis, D. P. (1989). "Laminar separating flow over a prolate spheroid." *Journal of Aircraft*, *26*(9), 810–816. https://doi.org/10.2514/3.45845

[11] Cox, R.N. and J.W. Maccoll, (1957). "Recent Contributions in Basic Hydroballistics," Proceedings of the Sympoisum on Naval Hydrodynamics, Publication 515, National Academy of Sciences – National Research Council, Washington DC.

[12] Dommermuth, D. G., O'Shea, T. T., Wyatt, D. C., Ratcliffe, T., Weymouth, G. D., Hendrikson, K. L., Yue, D. K., Sussman, M., Adams, P. and Valenciano, M. (2007)."An Application Of Cartesian-Grid And Volume-Of-Fluid Methods To Numerical Ship Hydrodynamics," Proc. of the 9th Int. Conf. on Numerical Ship Hydrodynamics, Ann Arbor, MI, August 5-8.

[13] Drazen, D., Beale, K.L.C., Bhushan, S., Fullerton, A.M., O'Shea, T., Brucker, K., Dommermuth, D., Wyatt, D., Carrica, P., Fu, T.C., Stern, F. (2010). "Comparisons of Model-Scale Experimental Measurements and Computational Predictions for the Transom Wave of a Large-Scale Transom Model,"

28th Symposium on Naval Hydrodynamics, Pasadena, CA, September 12-17.

[14] El Khoury, G. K., Andersson, H. I., & Pettersen, B. (2010). "Crossflow past a prolate spheroid at Reynolds number of 10000." *Journal of Fluid Mechanics*, 659, 365–374. https://doi.org/10.1017/S0022112010003216.

[15] Faltinsen, O. (2005). Hydrodynamics of High-Speed Marine Vehicles, Cambridge University Press, New York.

[16] Fu, T. C., Fullerton A.M., Terrill E. and Lada G. (2006). "Measurements of the Wave Field around the *R/V Athena I,"* 26th Symposium on Naval Hydrodynamics, Rome, Italy, September 17-22.

[17] Fu, T. C., Karion, A., Pence, A.M., Rice, J.R., Walker, D. & Ratcliffe, T. (2005). "Characterization of the Steady Wave Field of the High Speed Transom Stern Ship – Model 5365 Hull Form." Naval Surface Warfare Center, Carderock Division, Hydromechanics Direct. R&D Report, NSWCCD-50-TR-2005/046, Aug. pp. 34.

[18] Fu, T.C, O'Shea, T.T., Brucker, K.A., Judge, C.Q., Ikeda, C.M., Wyatt, D.C., and Dommermuth, D.G. (2014). "Numerical Simulation of Short Duration Hydrodynamic Impact," 33rd International Conf. on Ocean, Offshore & Arctic Engineering (OMAE2014), San Francisco, CA, USA, OMAE2014-24323, June 8-13.

[19] Fu, T.C., O'Shea, T.T., Judge, C.Q., Dommermuth, D.G., Brucker, K., and Wyatt, D.C. (2012). "A Detailed Assessment of Numerical Flow Analysis (NFA) to Predict the Hydrodynamics of a Deep-V Planing Hull," Proceedings of the 29th Symposium on Naval Hydrodynamics, Gothenburg, Sweden, August 26-31.

[20] Fu, T.C., Ratcliffe, T., O'Shea, T., Brucker, K., Graham, R., Wyatt, D., & Dommermuth, D. (2010). "A Comparison of Experimental Measurements & Computational Predictions of a Deep-V Planing Hull," Proceedings of the 28th Symposium on Naval Hydrodynamics, Pasadena, CA, September 12-17.

[21] Fu T. C., Shekarriz A., Katz J., Huang T. T. (1994). "The flow structure in the lee of an inclined 6:1 prolate spheroid," *J. Fluid Mech.* 269, 79–106, https://doi.org/10.1017/S0022112094001497

[22] Fureby, C., & Norrison, D. (2019). "RANS, DES and LES of the Flow Past the 6:1 Prolate Spheroid at 10° and 20° Angle of Incidence." AIAA Scitech, January, 1–15. https://doi.org/10.2514/6.2019-0085

[23] Furey, D.A. and Fu, T.C. (2002), "Quantitative Visualization (QViz) Hydrodynamic Measurement Technique of Multiphase Unsteady Surfaces," 24th Symposium on Naval Hydrodynamics, Fukuoka, JAPAN, July 8-13.

[24] Gee, K., Cummings, R. M., & Schiff, L. B. (1992). "Turbulence model effects on separated flow about a prolate spheroid." *AIAA Journal*, 30(3), 655–664. https://doi.org/10.2514/3.10969

[25] Hoang, N., Wetzel, T., & Simpson, R. (1994). "Unsteady measurements over a 6:1 prolate spheroid undergoing a pitch-up maneuver." https://doi.org/10.2514/6.1994-197

[26] Hoang, N., Wetzel, T., & Simpson, R. (1994). "Surface pressure measurements over a 6:1 prolate spheroid

undergoing time-dependent maneuvers." https://doi.org/10.2514/6.1994-1908

[27] Jiang, F., Gallardo, J. P., & Andersson, H. I. (2014). "The laminar wake behind a 6:1 prolate spheroid at 45° incidence angle." *Physics of Fluids*, 26(11). https://doi.org/10.1063/1.4902015</p

[28] Jiang, F., Gallardo, J. P., Andersson, H. I., & Zhang, Z. (2015). "The transitional wake behind an inclined prolate spheroid." *Physics of Fluids*, 27(9). https://doi.org/10.1063/1.4929764

[29] Jiang, M., Lien, V., Lesar, D.E., Engle, A., and Lewis, R. (2012) "A Validation of Various Codes Using Hydrodynamic Wedge Impact Data," Proceedings of the 31st International Conference on Ocean, Offshore, & Arctic Engineering, Rio de Janeiro, BRAZIL, July 1-6.

[30] Karlsson A., Fureby F. C. (2009). "LES of the flow past a 6: 1 prolate spheroid." *Proceedings of the 47th AIAA Aerospace Sciences Meeting*, AIAA No. 2009-1616, pp. 1–13.

[31] Kim, S-E and Rhee, S.H. (2003). "Application of modern turbulence models to vortical flow around a 6:1 prolate spheroid at incidence." AIAA paper 2003-0429, 41st AIAA aerospace sciences meeting and exhibit, Reno NV.

[32] Lee, (2018). "Longitudinal development of flow-separation lines on slender bodies in translation." *Journal Fluid Mechanics*, Vol. 837, pp. 627-639.

[33] Lesar, D. E., Jiang, M., Lien, V., Engle, A. and Lewis, R. (2012). "Validation of Numerical Analysis Codes for Hydrodynamic Impact Simulation using Rigid Wedge Drop Test Data," draft NSWCCD Technical Report.

[34] Maki, K.J., Doctors, L.J., and Beck, R.F. (2007). "On the Profile of the Flow Behind a Transom Stern." *Ninth Int. Conf. on Numerical Ship Hydrodynamics*, Ann Arbor, MI.

[35] Martínez-Legazpi, P., Marugan-Cruz, C., Rodríguez-Rodríguez, J. and Lasheras, J.C. (2013). "Plunging to spilling transition in corner surface waves in the wake of a partially submerged vertical plate." *Experiments in Fluids*. 54:1437-1448.

[36] Mor-Yossef, Y. (2015). "Separated Flow Prediction Around a 6:1 Prolate Spheroid Using Reynolds Stress Models." Springer International Publishing Switzerland B. Eisfeld (ed.), *Differential Reynolds Stress Modeling for Separating Flows in Industrial Aerodynamics*, Springer Tracts in Mechanical Engineering, DOI 10.1007/978-3-319-15639-2_3.

[37] O'Shea, T. T., Brucker, K. A., Dommermuth, D. G. and Wyatt, D. C. (2008). "A Numerical Formulation for Simulating Free-Surface Hydrodynamics," Proceedings of the 27th Symposium on Naval Hydrodynamics, Seoul, Korea, Oct. 5-10.

[38] Rhee, S. H., & Hino, T. (2002). "Numerical simulation of unsteady turbulent flow around maneuvering prolate spheroid." *AIAA Journal*, 40(10), 2017–2026. https://doi.org/10.2514/3.15291

[39] Saeidinezhad, A., Dehghan, A.A., and Manshadi, M.D. (2015), "Nose shape effect on the visualized flow field around an axisymmetric body of revolution at incidence," *J. of Visualization*, 18(1), 83-93, DOI: 10.1007/s12650-014-0226-1.

[40] Strandenes, H., Jiang, F., Pettersen, B., & Andersson, H. I. (2019). "Near-Wake of an Inclined 6:1 Spheroid at Reynolds Number 4000." *AIAA Journal*, 57(4), 1364–1372. https://doi.org/10.2514/1.j057615

[41] Terrill, E.J., and Fu, T.C. (2008) "At-Sea Measurements for Ship Hydromechanics," (*Invited paper*) to the 27th Symposium on Naval Hydrodynamics, Seoul, Korea, October 5-10.

[42] Wetzel T. G., Simpson R. L., Chesnakas C. J. (1998). "The measurement of 3D crossflow separation," *AIAA J.* 36, 557-564, https://doi.org/10.2514/3.13861

[43] Wetzel, T. G., & Simpson, R. L. (1998). "Unsteady crossflow separation location measurements on a maneuvering 6:1 prolate spheroid." AIAA Journal, 36(11), 2063–2071. https://doi.org/10.2514/3.14086

[44] Wikström, N., Svennberg, U., Alin, N., & Fureby, C. (2004). "Large eddy simulation of the flow around an inclined prolate spheroid." *Journal of Turbulence*, 5. https://doi.org/10.1088/1468-5248/5/1/029

[45] Wilson, W., Fu, T.C., Fullerton, A.M., & Gorski, J. (2006), "The Measured & Predicted Wave Field of Model 5365: An Evaluation of Current CFD Capability," 26th Symp. on Naval Hydro., Rome, Italy, Sept. 17-22.

[46] Wyatt, D.C. (2000). "Development and Assessment of a Nonlinear Wave Prediction Methodology for Surface Vessels," *Journal of Ship Research*, Vol. 44, No. 2, pp. 96-107.

[47] Wyatt, D.C. and Dommermuth D.G. (2006), "Semi-Empirical Prediction of Breaking Stern Waves," 26th Symposium on Naval Hydrodynamics, Rome, Italy, September 17-22.

[48] Wyatt, D.C., Fu, T.C., Taylor, G.L., Terrill, E.J., Xing, T., Bhushan, S., O'Shea, T.T., and Dommermuth, D.G. (2008), "A Comparison of Full-Scale Experimental Measurements and Computational Predictions of the Transom-Stern Wave of the R/V Athena I," 27th Symposium on Naval Hydrodynamics, Seoul, Korea, October 5-10.